BIBECHANA
Vol. 23, No. 2, April 2026, 100-114

ISSN 2091-0762 (Print), 2382-5340 (Online)
Journal homepage: http://nepjol.info/index.php/BIBECHANA
Publisher:Dept. of Phys., Mahendra Morang A. M. Campus (Tribhuvan University)Biratnagar

Seismo-ionospheric coupling of two shallow and moderate earthquakes in Indonesia in 2024 observed via TEC analysis

Madhu Sudan Paudel[1, 2*], Basu Dev Ghimire[3], Narayan Prasad Chapagain[4]

[1]*Department of Physics, Tri-Chandra Multiple Campus, Tribhuvan University, Nepal.*
[2]*Central Department of Physics, Tribhuvan University, Kirtipur, Nepal.*
[3]*Department of Physics, St. Xavier's College, Tribhuvan University, Nepal.*
[4]*Department of Physics, Amrit Campus, Tribhuvan University, Nepal.*

*Corresponding authors: Email: mspaudel27@gmail.com;madhu.paudel@trc.tu.edu.np

Abstract

This study investigates the seismo-ionospheric coupling associated with two magnitude 6.4 (M6.4) earthquakes that occurred in Indonesia in 2024: the March 22 event near Paciran (5.875° S, 112.365° E) and the April 9 event near Tobelo (2.698° N,127.062° E). Data from GNSS permanent ground stations BNOA and BTNG, obtained from UNAVCO, were used to analyze temporal variation in the ionospheric Total Electron Content (TEC) before and after the earthquakes. The spatiotemporal variations of the TEC were studied using the Global Ionospheric Map of TEC (GIM-TEC) data. A running quartile-based method was applied to estimate the upper bound (UB) and lower bound (LB) of TEC in order to identify anomalous variation. The geomagnetic indices were also studied in order to segregate anomalies associated with space weather condition. The difference of TEC (dTEC) map from GIM-TEC revealed simultaneous negative and positive anomalies in magnetically conjugate regions of the Equatorial Ionospheric Anomaly (EIA), beginning 6 days prior to the Paciran earthquake and 11 days prior to the Tobelo earthquake. The negative TEC anomalies were also accompanied by morphological changes in the EIA profile. The observed positive and negative anomalies are interpreted in terms of radon emanation mechanism associated with pre-earthquake Lithosphere-Atmosphere-Ionosphere Coupling (LAIC).

Keywords
*S*eismo-ionospheric coupling; GNSS; Ionospheric TEC; GIM-TEC; EIA.

Article information
Manuscript received: February 10, 2026; Revised: April 17, 2026; Accepted: April 26, 2026
DOI https://doi.org/10.3126/bibechana.v23i2.90756

1 Introduction

Earthquake represent one of the most devastating natural disasters prevailing all over the world, mostly concentrated at boundaries of the tectonic plates. It causes significant loss of human life and infrastructure. Understanding the physical processes underlying behind the seismo-ionospheric coupling mechanism and identifying the reliable precursory signature are crucial for earthquake monitoring and early warning systems. Hayakawa (1994, 2006) [1, 2] suggested Lithosphere – Atmosphere – Ionosphere Coupling (LAIC) mechanism, which involves the emission of various types of waves before and during the earthquakes. The low frequency electromagnetic wave, gravity wave, acoustic gravity wave are the examples of such waves. These waves can significantly modify the electric field associated with the Global Electric Circuit (GEC), leading to changes in the ionization rates in the ionosphere. These waves are distinct from the seismic waves that are responsible for ground movement, such as Primary (P), Secondary (S), and Raleigh waves. There is an alternative and widely discussed model of LAIC mechanism based on the radioactive radon emanation prior to earthquake. The release of radon in atmosphere ionizes the air molecules, altering the air conductivity near the surface around the epicenter. This change affects the GEC and modifies the ionospheric potential relative to ground [3–7].

In the early stages, studies of seismo-ionospheric coupling primarily relied on the anomalies in critical frequency of the F2 layer of ionosphere (foF2) [8]. With the development of the Global Positioning System (GPS) and other Global Navigation and Satellite System (GNSS), it has become possible to study the ionospheric Total Electron Content (TEC) variations with improved spatial and temporal resolution [9]. The variations of ionospheric TEC before several earthquakes having magnitude greater than 6.0 has been studied using quartile-based threshold method, where TEC anomalies observed under geomagnetic quiet conditions are often considered potential earthquake precursors. However, the occurrence of pre-earthquake anomaly days has not been consistent among different events. For example, anomalies were reported 5 days before for 16 earthquakes among 20 under study in Taiwan between 1999 to 2002 [10], 3-5 days before 17 earthquakes in China between 1998 to 2008 [11], 9 days before magnitude 7.7 (M7.7) Chile earthquake on November 14, 2007 [12], 3 days before in M7.8 Gorkha earthquake in Nepal on April 25, 2015, 5 days before M7.3 earthquake in Nepal on May 12, 2025, 10 days before M7.8 earthquake in Iran-Iraq border on November 12, 2017 [13], 1 and 9 days before M7.8 Gorkha earthquake in Nepal on April 25, 2015 [14], 5-10 days before and 5 days after in M8.2 earthquake in Fiji on August 19, 2018 [15], 6 days before M6.8 earthquake in Morocco on September 8, 2023 [16], 3 days before Pakistan M7.7 earthquake on September 24, 2024 [17], etc. The lack of a comprehensive physical model capable of fully explaining pre-earthquake ionospheric precursor remains a major challenge in this field. Therefore, the investigation of additional earthquake events and their associated TEC anomalies is essential for improving the understanding of underlying physical mechanism.

In low-latitude regions, ionospheric TEC anomalies in are strongly influenced by the Equatorial Ionization Anomaly (EIA). In most cases, TEC anomalies are observed a few days to about a week before the earthquakes [18–20]. The positive or negative anomalies are often distributed across the both the EIA crests in magnetically conjugate region due to fountain effect, rather than being confined to the vicinity of the epicenter. Moreover, the morphology of the EIA curve has been reported to be distorted several days to week before [20], often accompanied by the equatorward movement of the EIA crest.

In this work, two earthquakes that occurred in Indonesia in 2024 were selected, both having moderate magnitude 6.4 (M6.4). The events are separated by 18 days, with epicenter distance 1579.631 km. The first earthquake occurred on March 22, 2024 near Paciran of Indonesia, while the second occurred on April 9, 2024 near Tobelo of Indonesia. Both seismic events have shallow hypocenter depth, earlier 9.5 km and later 22.0 km. The basic information about the both earthquakes is summarized on Table 1.

Table 1: Basic information about the earthquakes under study. Both earthquakes have magnitude 6.4. Source: USGS (https://earthquake.usgs.gov/earthquakes/)

Date	Epicenter	Latitude	Longitude
March 22, 2024	Paciran, Indonesia	5.875°S	112.365°E
April 9, 2024	Tobelo, Indonesia	2.698°N	127.062°E

The objective of this study is to investigate the ionospheric TEC anomalies associated with two M6.4 earthquakes in Indonesia using GNSS and GIM-TEC data. The observed anomalies before and after both earthquakes will be compared. Section 2 describes the materials and methods; Section 3 presents the results and discussions and Section 4 presents the conclusions.

2 Materials and Methods

2.1 Sources of Data

The Receiver Independent Exchange (RINEX) file containing the information of the pseudo range of the GNSS signal is used to estimate the ionospheric TEC. The GNSS stations within the Earthquake Preparation Zone (EPZ), as given by Dobrovolsky radius $R = 10^{-0.43M}$, are selected, where M is the magnitude of earthquake [21]. For M = 6.4, R will be 564.937 km. Only one active GNSS station lies within the radius of EPZ for each earthquake, with station BNOA near the Paciran earthquake and station BTNG near the Tobelo earthquake, as shown in Fig. 1. The RINEX data are downloaded from March 2 to April 19, 2024 for both stations BNOA and BTNG from UNAVCO. The detail information of the longitude, latitude, altitude and distance of the GNSS stations from epicenter is given in Table 2. The distance of GNSS stations is measured from corresponding epicenters of earthquake. Vincentry's formula [22] was used to estimate the distance between epicenter and GNSS station, which is based on the World Geodetical System 84 (WGS 84) and very appropriate for the geodesy.

The Global Ionospheric Map of TEC (GIM-TEC) was taken from the International GNSS Service (IGS) having 1-hour temporal resolution and 2.5° × 5.0° spatial resolution along latitude and longitude. This much resolution is sufficient to distinguish the anomalies in TEC cloud over the earthquake preparation zone. The GIM-TEC data consists of total (71 × 73) grids for whole globe. But we have used only the region between the latitude (25° S to 35° N) and longitude (70° E to 180° E). This much range of latitude and longitude is sufficient to include the earthquake preparation zone and both crest of EIA so that any spatial TEC anomalies observed around the EPZ and EIA crests could be seen clearly.

Table 2: Geographical latitude, longitude, altitude of GNSS station and distance of GNSS stations from epicenter of respective earthquake are given in table.

GNSS Station	Latitude	Longitude	Altitude	Distance
BNOA	8.747°S	115.211°E	39.1 km	446.787 km
BTNG	1.439°N	125.193°E	75.0 km	502.516 km

Table 3: The geomagnetic quiet (Q) and disturbed (D) days of the March and April of 2024 is given below. The days are arranged in the order of most effective to less effective. Source: https://isgi.unistra.fr/data_download.php

Month (2024)	10 Q - days: Q1, Q2, Q3, Q4, Q5, Q6, Q7, Q8, Q9, Q10	5 D - days: D1, D2, D3, D4, D5
March	17, 16, 30, 11, 20, 18, 2, 29, 12, 6	24, 23, 3, 25, 21
April	25, 24, 18, 14, 12 11, 13, 3, 29, 28	19, 16, 26, 21, 30

2.2 Estimation of Ionospheric TEC

TEC is defined as the line integral of the number density of electron along the cylindrical path having unit cross section area. If we assume the path from satellite transmitter (Tx) to ground receiver (Rx), then,

$$TEC = \int_{Rx}^{Tx} N_e dl \tag{1}$$

where, N_e is electron density, dl = differential path Ionosphere is a conductive medium, hence it is dispersive for the electromagnetic signal (GNSS signal). The refractive index (η) of the ionosphere can be written in terms of the frequency and electron density [23].

$$\eta = 1 - \frac{40.3}{f^2} N_e \tag{2}$$

The path delay due to the refraction depends on the frequency of GNSS signal. In fact, the path delay (δr) introduced by ionosphere due to refraction is inversely proportional to its frequency, given as;

$$\delta r = \frac{40.3}{f^2} \int_{Rx}^{Tx} N_e dl = \frac{40.3}{f^2} TEC \tag{3}$$

The pseudo-range of the GNSS signal can be written as;

$$P = R + \delta r + \Sigma errors \quad (4)$$

where, R is geometrical range and Σerrors includes the tropospheric delay, delay due to satellite and receiver clock, ephemeris error, error due to multipath and noise. These all errors are independent to the frequency of GNSS signal.

For GNSS signal at two frequencies; f1 (for L1, 1575.42 MHz) and f2 (for L2, 1227.60 MHz), we can write equation (4). If we subtract the equation, we get,

$$P_1 - P_2 = \delta r_1 - \delta r_2 \quad (5)$$

Using equation (3) in (5), we can estimate the TEC as;

$$TEC = \frac{1}{40.3}\left[\frac{f_1^2 \times f_2^2}{f_2^2 - f_1^2}\right](P_1 - P_2) \quad (6)$$

The TEC calculated along the path of GNSS signal in ionosphere is known as the slant TEC (STEC). The STEC is not relevant to describe the actual behavior of the ionosphere. It can be converted to the vertical TEC (VTEC) using the proper geometrical conversion. The Fig. 1 describes the necessary geometry for the conversion of STEC to VTEC based into Single Layer Model (SLM) of ionosphere.

The VTEC can be estimated from from STEC using mapping function (S(E)), gives as [24, 25];

$$VTEC = [STEC - c(DCB^s + DCB_r)] \times S(E) \quad (7)$$

where, DCB is differential code bias and the prefix s and r indicates satellite and receiver, c is the speed of light.
The mapping function S(E) is given as;

$$S(E) = \sqrt{1 - \left(\frac{R_e}{R_e + h_{ipp}} \cos(E)\right)^2} \quad (8)$$

Where, h_{ipp} is the height of the ionospheric pierce point, R_e is the radius of earth, E is elevation angle of the satellite with respect to user. The value of h_{ipp} and R_e are taken 350 km and 6378 km respectively [25].
The value of VTEC is computed from RINEX file containing pseudo range P1 and P2 at frequency f1 and f2, using GPS-TEC analysis program version 3.5 [25], downloaded from personal blog of Gopi Seemala (https://seemala.blogspot.com/).

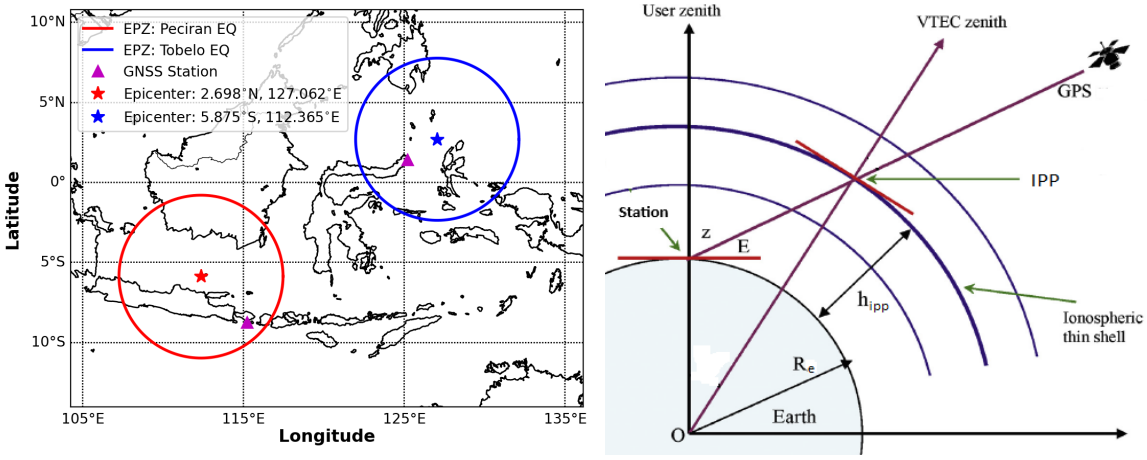

Figure 1: Left: Map of the region around the epicenter of both earthquake can be seen. The GNSS stations are indicated by inverted triangle. The EPZ is represented by circle around both earthquake. Right: Geometry for the conversion of STEC to VTEC based on SLM ionospheric model [25].

2.3 Detection of Anomalies in VTEC

One of the major tasks to achieve the objective of this research work is to identify the anomalies in ionospheric VTEC before and after the earthquake day. A running quartile-based method was used to estimate the upper bound (UB) and lower bound (LB) of VTEC in order to detect anomalous deviations from the background ionospheric behavior following [8, 10, 26]. The data set of each hour from previous 30 day was taken to compute the median (M), lower quartile (LQ) and upper quartile (UQ). The lower bound (LB) and upper bound (UB) of ionospheric VTEC for 31th day were estimated using formula;

$$\begin{aligned} LB &= M - 2.0(M - LQ) \\ UB &= M + 2.0(UB - M) \end{aligned} \quad (9)$$

If the observed VTEC lies beyond either LB of UB as defined by equation (9), then it is declared as anomaly in VTEC. The number 2.0 is chosen for threshold so as to fix the confidence level $\sim$ 82 % [27].

The difference of TEC (dTEC) between the VTEC and either LB or UB is estimated using following expression [18, 20];

$$dTEC = \begin{cases} VTEC - UB, & \text{if UB} \geq \text{VTEC (+ve)} \\ 0, & \text{if LB} < \text{VTEC} < \text{UB} \\ VTEC - LB, & \text{if VTEC} < \text{LB (-ve)} \end{cases} \quad (10)$$

2.4 GIM-TEC and Map dTEC

The GIM-TEC was used to construct the map of difference of TEC (dTEC). It consists of grided data with a spatial resolution 2.5° × 5.0° in latitude and longitude, and a temporal resolution of 1 hour. For each grid and a given hour, the monthly median (M) was estimated using the TEC data from preceding 30 days. The dTEC for 31^{th} day was obtained by subtracting the median TEC (M) from the TEC value on that day for same grid and hour. Using this approach, dTEC map were generated to analyze the spatiotemporal variations of TEC anomalies. The GIM-TEC was also used to extract the TEC at the position near the epicenter of both earthquakes to study the temporal variation within the studied time window.

2.5 Space Weather Filtering Criteria

The space weather is a crucial driver for ionospheric TEC. In this study, we examine the geomagnetic and solar indices, such as Dst index, Kp index, SSN and F10.7 index, in order to investigate the possible connection between TEC anomalies with space weather conditions. The threshold values of geomagnetic indices are defined as follows: for a moderate storm, Dst $<$ -50 nT and Kp $>$ 4; for a strong storm, Dst $<$ -100 nT and Kp $>$ 6; and for a super storm, Dst $<$ -200 nT and Kp $>$ 8 [28].

Similarly, the threshold values for solar indices are defined as follows: for a moderate solar activity, SSN $>$ 50 and F10.7 $>$ 100 sfu; for a high solar activity, SSN $>$ 100 and F10.7 cm $>$ 150; and for an extreme solar activity, SSN $>$ 200 sfu and F10.7 cm $>$ 200 sfu [29–31]. In addition to these indices, the geomagnetic quiet days (Q-days) and disturbed days (D-days) were also considered for the identification of TEC anomalies associated with the earthquakes. The criteria for the selection of geomagnetic D and Q days are described in Matzka et al., (2021) [32].

3 Results and Discussion

3.1 Temporal Variation of VTEC and GIM-TEC

The temporal variation of the TEC before and after Paciran earthquake, from March 1, 2024 to April 4, 2024 is shown in Fig. 2. Fig. 2 (a) represents the VTEC from the ground station BNOA and Fig. 2(b) represents the TEC extracted from GIM-TEC data at the epicenter of the Peciran earthquake. In each figure, the lower panel shows the histogram of the dTEC, which has positive and negative value for respective anomalies. The colors are assigned to represent the geomagnetic conditions; green for Q-days, red for D-days and black for normal days. If a TEC anomaly is observed continuously for three or more hours, the day is considered an anomaly day. Based on this criterion several anomaly days are identified, which are presented in Table 4.

The anomalies are observed before 20 days up to after 11 days of the earthquake day in both VTEC and GIM-TEC data. In VTEC data, anomalies are observed sharp and continuous compare to GIM-TEC. In many days, we can see the anomalies in both data but on March 11, anomaly can be observed in VTEC data. The anomalies observed on D-days, such as March 21, 24, 25 are equally effective on both VTEC and GIM-TEC data because of space weather effect. The anomalies in TEC on March 2, 4, 23, 26, April 2 and 4 are observed on both data most effectively, which are before 20 and 18 days of earthquake and 1, 4, 11 and 12 days after the earthquake.

The temporal variation of the TEC before and after Tobelo earthquake, from March 19, 2024 to April 18, 2024 is shown in Fig. 3. Fig. 3 (a) is for the VTEC from ground station BTNG and Fig. 3(b) is for TEC extracted from GIM-TEC near the epicenter of Tobelo earthquake. In both data, TEC anomalies can be observed in similar pattern continuously from March 19 to 27, and on April 2, 4, 8, 13, 16, 17, and 18. In April 2, positive anomalies are observed in VTEC from BNOA station and negative anomalies from BTNG station. This could be associated with localized effects, in which earthquake is one of the possible causes.

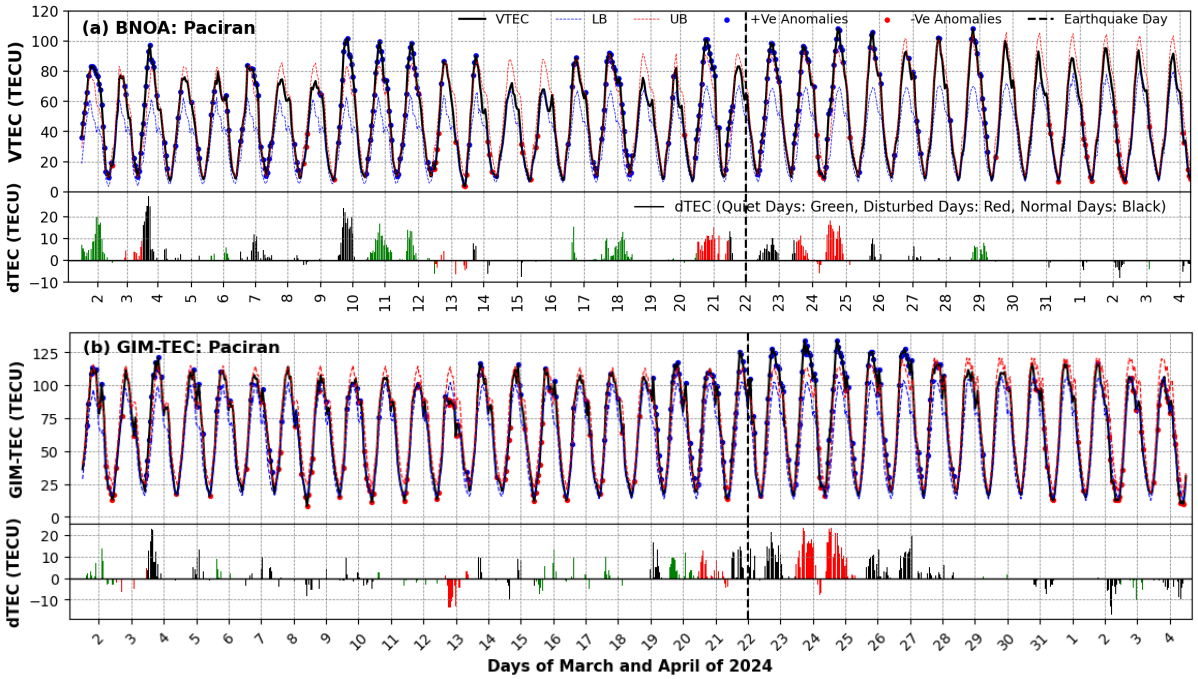

Figure 2: The temporal variation of the TEC together with UB and LB from March 2, 2024 to April 4, 2024 can be seen. Figure (a) is for VTEC from BNOA station and figure (b) is for TEC from GIM.

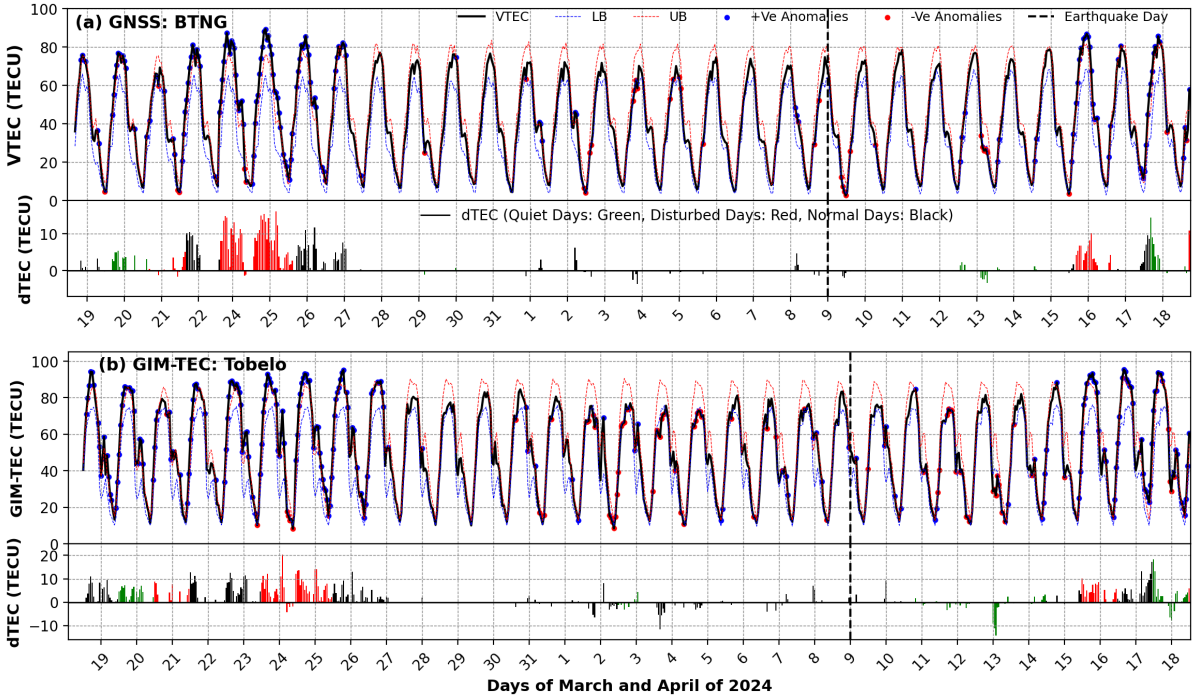

Figure 3: The temporal variation of the TEC together with UB and LB from March 19, 2024 to April 18, 2024 can be seen. Figure (a) is for VTEC from BTNG station and figure (b) is for TEC from GIM.

In both earthquakes, the anomalies in TEC are observed on geomagnetic quiet, normal and disturb days. The anomaly in geomagnetic disturb days might be associated with the space weather conditions. From March 22 to 27, anomalies can be observed from both BONA and BTNG stations. This might be the effect of space weather. On March 10, 11, 12, 18 and 29, the anomaly is observed only in BNOA station data, and cannot be observed in BTNG data. Likewise, on March 20, April 2, 8, and 13 the anomalies can be seen from GNSS station BTNG but not from BNOA station data. The data

Table 4: The anomaly day corresponding to different geomagnetic condition before and after the both Paciran and Tobelo earthquakes.

Earthquake	Geomagnetic Condition	Anomaly Days
Peciran	Quiet days	March 2, 11, 12, 17, 18, 29
	Normal days	March 4, 7, 10, 14(-ve), 22, 23, 26 April 2, 4
	Disturbed days	March 21, 24, 25
Tobelo	Quiet days	March 20, April 2, 4 (-ve), 8, 13 (-ve), 18
	Normal days	March 19, 22, 23, 26, 27, April 5(-ve), 17
	Disturbed days	March 21, 24, 25, April 16

before March 18 at the BTNG stations and after April 4 at the BNOA station are excluded from the respective graph. The TEC anomalies confined to GNSS stations within EPZ indicate an association with local terrestrial factor, such as nearby earthquake. The anomaly day according to the geomagnetic quiet, normal and disturb days is presented in Table 4. As the epicenters of both earthquakes are located in low-latitude regions, TEC anomalies are expected in the EIA and magnetically conjugate regions. The spatiotemporal variation of TEC anomalies in EIA region is presented the following section.

3.2 Variation of Geomagnetic and Solar Indices

The temporal variations of geomagnetic indices (Dst and Kp) and solar indices (F10.7 and SSN) are studied from March 2 to April 19, 2024, are analyzed, as shown in Fig. 4. This date covers the time frame of the both earthquakes. The horizontal lines represent the threshold values of respective indices, while the vertical lines indicate the earthquakes on March 22 (Paciran) and April 9 (Tobelo).

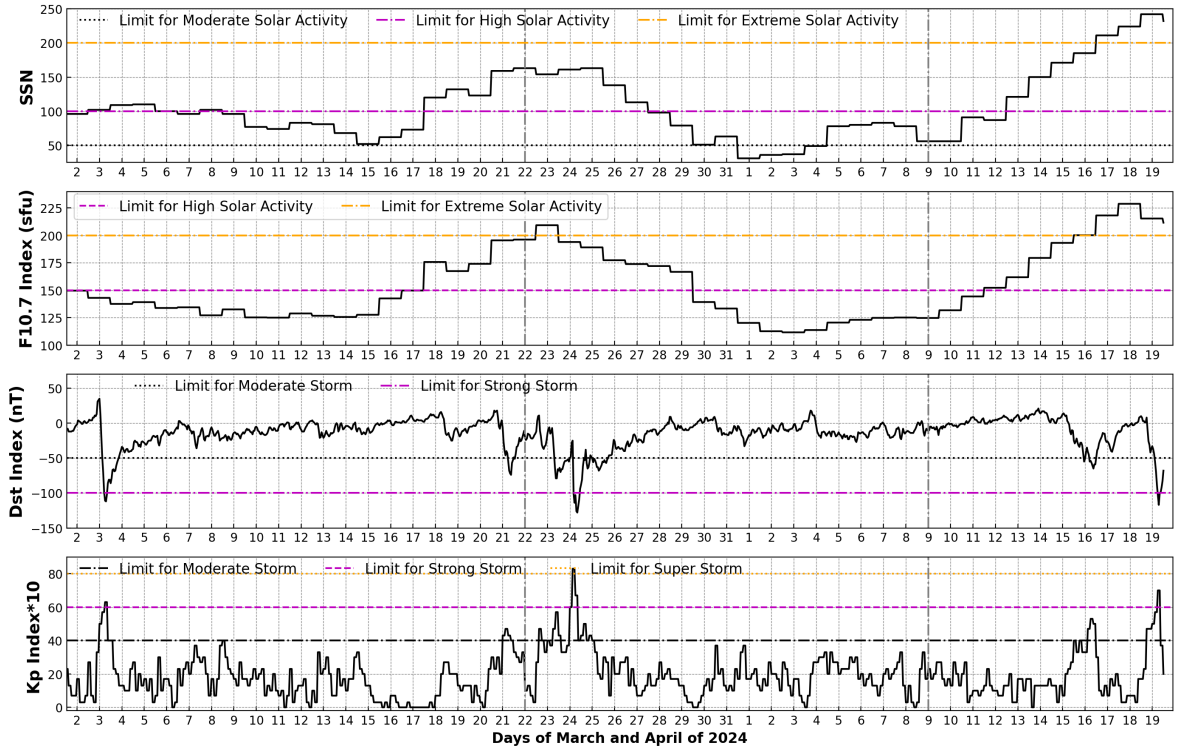

Figure 4: Solar and geomagnetic indices; SSN, F10.7 index, Kp index and Dst index panel from March 2, 2024 to April 19, 2024. Vertical dotted lines represent earthquake day on March 22 and April 9.

Geomagnetic indices indicate strong storm conditions on March 3, 24 and April 19, with Kp > 6 and Dst < - 100 nT, and moderate storm conditions on March 21, 23, 25, April 16, with Kp > 4 and Dst < - 50 nT. These days also belongs to geomagnetic D - days of this month.

From March 21-25, the SSN exceeds 150 and F10.7 index reaches ∼ 200 sfu, with a maximum on March 23. Similarly, during April 14-19, SSN increases above 150 and F10.7 surpasses 175 sfu. The elevated solar indices correspond to an increase in the diurnal peak TEC, resulting in positive TEC anomalies. However, moderate storm conditions on March 21 and a strong storm on March 24 may also have contributed to these positive anomalies. The Paciran earthquake on March 22 belongs to the date when solar activity is high and quiet geomagnetic condition whereas the Tobelo earthquake on April 9 belongs to moderate solar activity and quiet geomagnetic condition.

3.3 Spatiotemporal Variation of dTEC in EIA Zone

The epicenters of both earthquakes lie in low-latitude regions where EIA is prominent. To investigate the pre-earthquake effect on the EIA, the spatiotemporal variation of the ionospheric TEC was analyzed using the GIM-TEC data. The TEC and dTEC map are prepared for each day within the study period. The EPZs of the both earthquakes are located near the southern crest of the EIA. The anomaly effect is expected to be observed at both EIA crests, including the magnetically conjugate region, rather than being confined only to the EPZ. Pulinets, (2008) [20] suggested enhancement of the positive TEC anomalies in the west of epicenter and its movement eastward after few days. Moreover, the negative TEC anomalies are accompanied by the morphological change in EIA profile.

On normal days, positive TEC anomalies are observed over EIA crest and negative anomalies over EIA trough, shifting from east to west as the EIA evolves across the study region. However, an opposite pattern is observed in some days preceding both earthquakes. Negative TEC anomalies can be observed over both EIA crests on March 16 and 19, corresponding to 6 and 3 days before of Paciran earthquake (March 22). In addition, positive anomalies appear west of epicenter on March 17 and 18, from 04:00 UT (11:00 LT) to 15:00 UT (22:00 LT). The anomaly pattern shows minimal westward movement during the afternoon hours as the EIA stabilizes. On March 19 and 21 positive anomalies are observed on the east of the epicenter, from 09:00 UT (16:00 LT) to 15:00 UT (22:00 LT). However, March 21 is geomagnetic D-days with moderate storm conditions (Kp $>$ 4 and Dst $<$ -50 nT). On March 19, both negative and positive anomalies are evident (Fig. 5), with negative anomalies near epicenter longitude and positive anomalies to the east. No significant anomalies are observed in dTEC map prior 16 March.

Prior to the Tobelo earthquake, a similar spatiotemporal TEC signature is observed, as shown in Fig. 6 On March 30, 11 days before Tobelo earthquake, a positive anomaly is observed west of the epicenter throughout the EIA active hours. This anomaly shifts to the east side after 3 days, appearing on April 2, which is 7 before days of the earthquake.

The negative anomalies are observed over the magnetically conjugate region of both EIA crests, accompanied by positive anomalies over the EIA trough on April 1, 3, 5, 8 and 9. On April 7, a positive TEC anomaly appears over the EIA crests near the epicenter longitude, between 07:00 UT (14:00 LT) to 13:00 UT (20:00 LT). The persistent occurrence of these positive and negative anomalies over extended hours in the low-latitude EIA region may represent signatures for the impending earthquakes.

3.4 Dynamics of EIA Prior to Earthquake

The dTEC map reveal TEC anomalies in the magnetically conjugate regions over both the EIA crests and trough. Previous studies have reported morphological changes in the EIA and an equatorward shift of the EIA crests several days to week prior to strong earthquakes [20,33]. To examine this behavior, TEC variations were analyzed along latitudes from 30° S to 40° N at the fixed longitude of each epicenter. The latitudinal TEC variations before the earthquakes are shown in Fig. 7 (Paciran earthquake) and Fig. 8 (Tobelo earthquake).

The TEC variations were analyzed daily during the study period from March 1 to April 20, 2024. Figures include the selected days exhibiting either positive or negative TEC anomalies. For comparison, latitudinal TEC profiles from 7:00 UT to 9:00 UT (14:00 LT to 16:00 LT), corresponding to the peak EIA hours in study region, are presented. The EIA profile is found to be distorted and diminished on the days associated with the negative TEC anomalies compared to days with positive anomalies. Additionally, the asymmetry between the southern and northern EIA crest is evident on anomaly day.

Distortions in EIA profile are observed on March 16 and 19, corresponding to 6 and 3 days before the Paciran earthquake, and on April 1, 3, 5, 8 and 9, corresponding to 8, 6, 4, 1 and 0 days before the Tobelo earthquake. On these days, the EIA crests

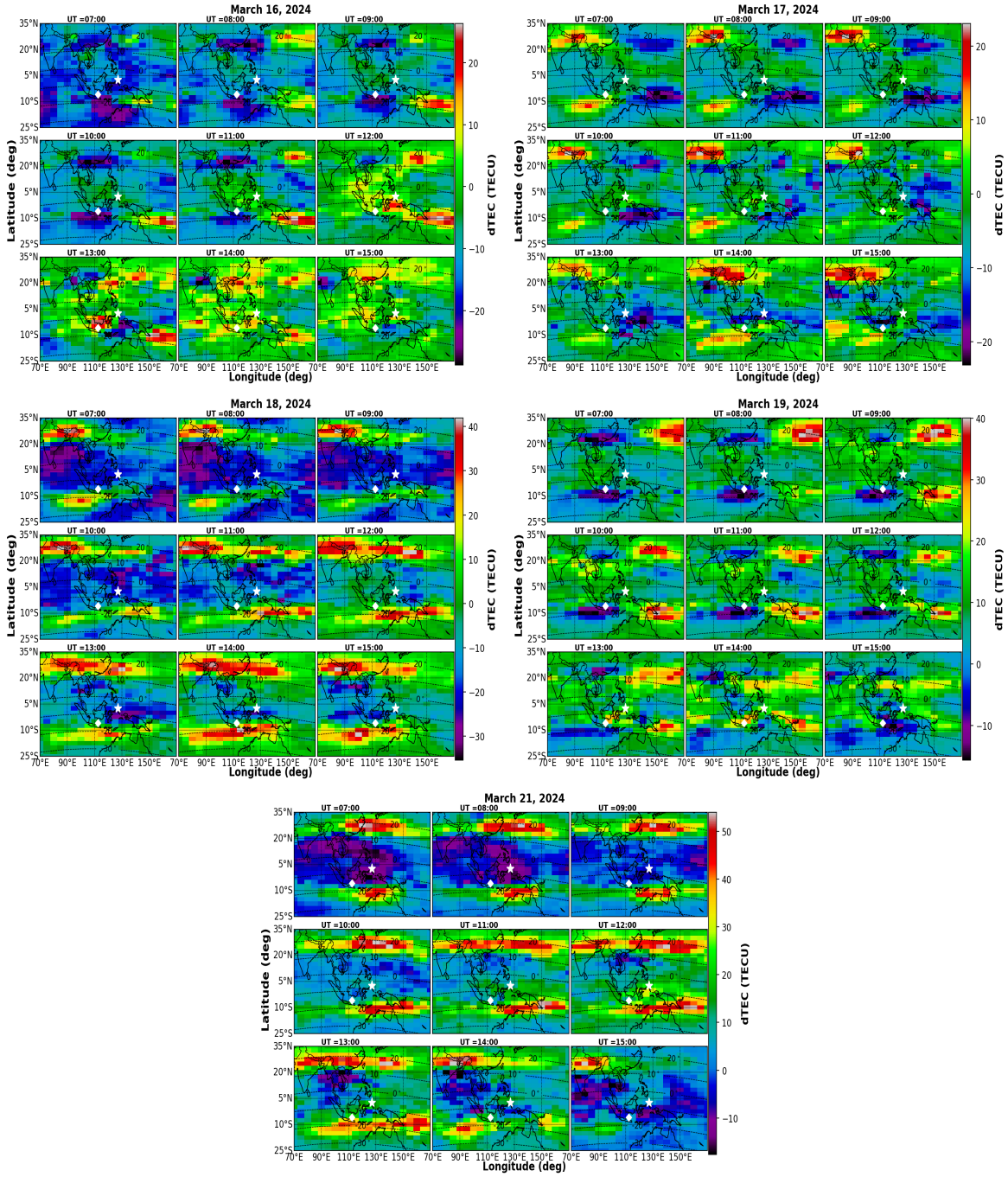

Figure 5: Map of dTEC on March 16, 17, 18, 19 and 21, from 7:00 UT to 15:00 UT. In this hour an active EIA can be observed in this study region. On March 16 and 19, negative anomaly can be seen in both crest of EIA. The positive anomaly in western part of epicenter can be seen on March 17-18, which shifts to eastern side on March 21. The epicenters of the earthquakes are indicated by white square (Paciran) and star (Tobelo) and dotted curved lines represent the geomagnetic latitude.

are weakened and shifted equatorward at 09:00 UT (16:00 LT). Similar behavior was reported three days before the M7.9 Wenchuan earthquake of May 12, 2008 [20, 33]. In contrast, on March 17, 18 and 21, corresponding to 5, 4 and 1 days before the Paciran earthquake, and on April 2 and 7, corresponding to 7 and 2 days before the Tobelo earthquake, the EIA crests shift poleward with enhanced TEC values compared to days associated with negative anomalies.

These variations in EIA dynamics are attributed to the interaction between background zonal electric fields and earthquake-induced anomalous electric field, providing evidence of seismo-ionospheric coupling prior to strong earthquakes in low latitude regions [33].

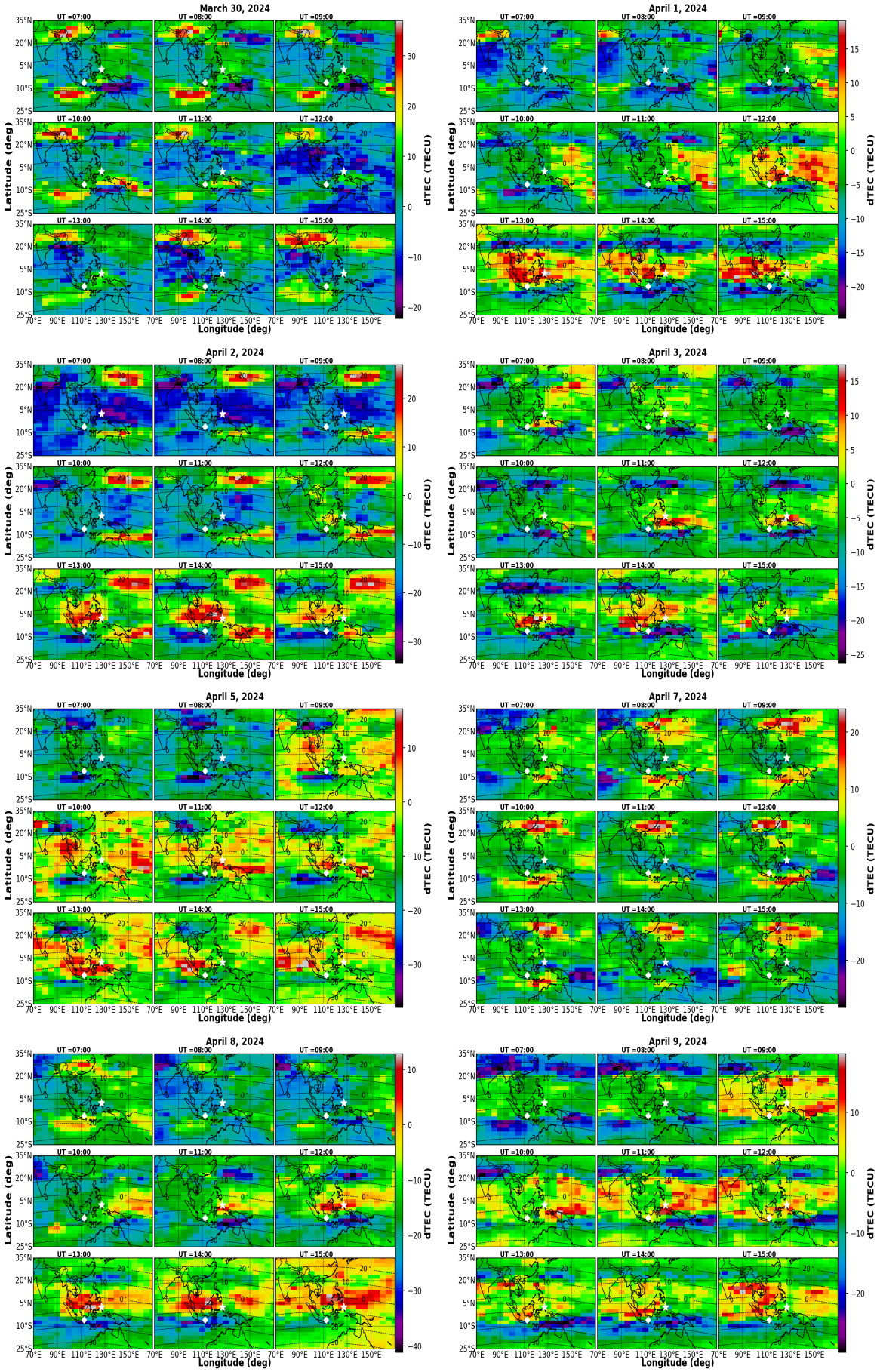

Figure 6: Similar to Fig. 5 but for March 30, April 1, 2, 3, 5, 8 and 9, from 7:00 UT to 15:00 UT. The positive anomaly can be seen in western side of epicenter (Tobelo) on March 30 and eastern side of epicenter on April 2. On April 1, 3, 5, 8 and 9 negative anomaly can be seen on the magnetically conjugate regions in EIA crests and positive anomaly in EIA trough positive anomaly on April 7.

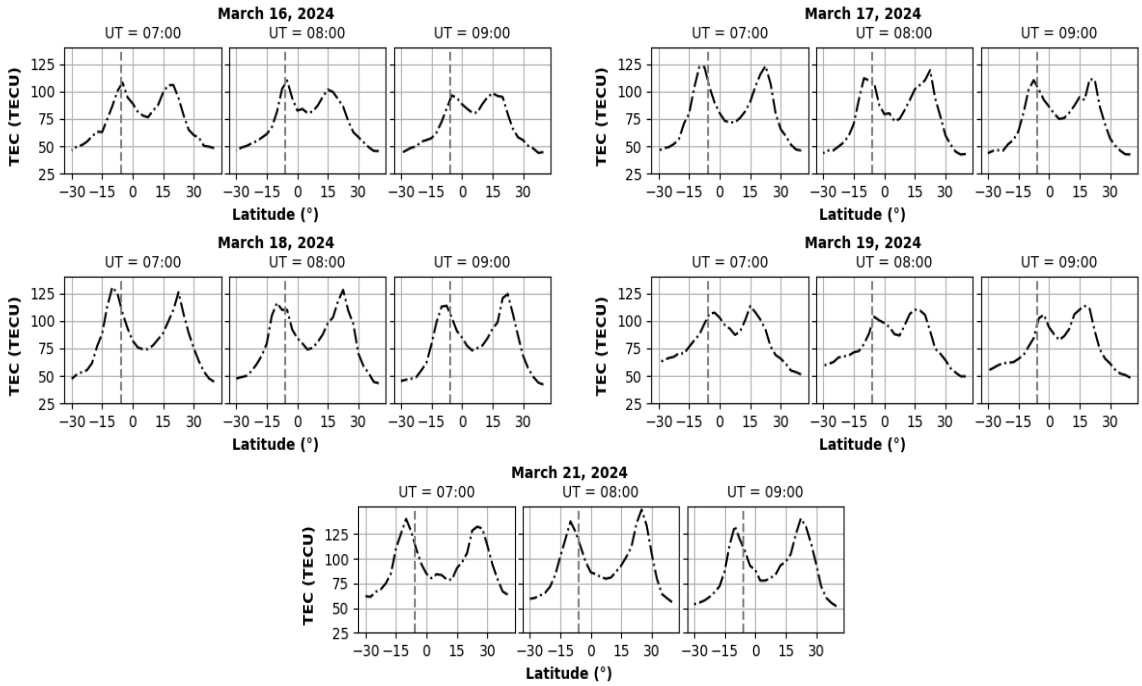

Figure 7: Latitudinal variation of TEC from 30° S to 40° N at fixed longitude of 112° E, corresponding to the Paciran earthquake epicenter, represented by vertical dashed line. Distortions in the EIA profile are observed March 16 and 19. Enhancement in TEC is observed on March 17, 18 and 21, corresponding to positive anomalies.

3.5 Discussion

The analysis of ionospheric TEC before and after the two shallow M6.4 earthquakes reveals the signatures of pre-seismic activity. The VTEC variations, evaluated using upper and lower bounds based on running quartiles method, show anomalies around the earthquake dates. The TEC enhancements are also observed during the geomagnetic storms; however, geomagnetically calm periods were identified to isolate the earthquake related anomalies. As both epicenters are located in low-latitude regions, corresponding effects are observed within the EIA. The dTEC maps reveal distinct spatiotemporal features prior to the earthquakes, including simultaneous anomalies in the magnetically conjugate regions of the EIA crests. Notably, negative anomalies over the EIA crests are often accompanied by positive anomalies in the trough region. This emphasize the importance of the regional variation of the ionospheric anomalies rather than globally. However, there might be inconsistency in observed anomalies at different regions as it strongly depends on the subsurface geology [34].

The observed spatiotemporal TEC anomalies can be interpreted within the framework of radon emanation model, in which radioactive gases such as radon are released from tectonic faults during the earthquake preparation phase [4, 6, 33]. The enhanced ionization near-surface air increases atmospheric conductivity within the EPZ, modifying the ionosphere-ground electric potential. This process generates anomalous electric field that alter vertical plasma drift through $\mathbf{E} \times \mathbf{B}$ mechanism, producing TEC anomalies around the epicenter. Initially, increased air conductivity enhances upward plasma drift west of EPZ, resulting the positive TEC anomalies in western sector. Subsequent hydration of ionized molecules reduces air conductivity and reverses the electric field polarity near EPZ. This process shifts the enhance upward drift eastward, leading to an eastward migration of positive TEC anomalies [33]. In this study, the west-to-east shift occurs within two days (March 19–21) before the Paciran earthquake and within three days (March 30–April 2) before the Tobelo earthquake, suggesting the conductivity changes over a 2–3 day timescale. The earthquake-induced anomalous electric field modifies the background zonal electric field, perturbing the $\mathbf{E} \times \mathbf{B}$ plasma drift, and consequently altering the EIA fountain effect. The reduced upward drift produces the negative TEC anomalies and weakens the fountain effect, resulting in distortion of the EIA profile and equatorward displacement of EIA crests. In contrast, enhanced upward drift strengthens the fountain effect, leading to poleward displacement of EIA crests during positive TEC anomalies. Similar morphological changes in EIA profile associ-

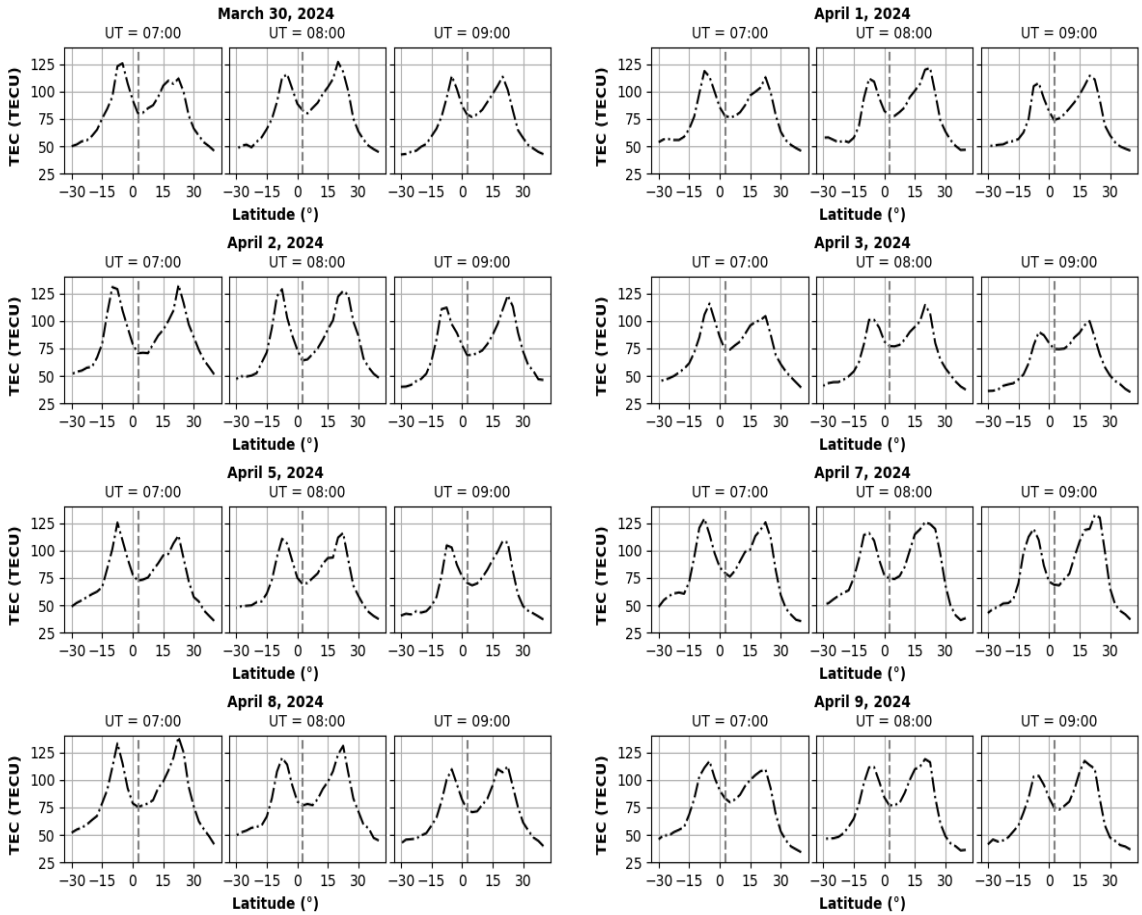

Figure 8: Same as Fig. 7, but before Tobelo earthquake at longitude 127° E. Maximum distortion in EIA crest is observed on April 1, 3, 5, 8 and 9.

ated with conjugate TEC anomalies have been reported prior to several major earthquakes, including the M9.1 earthquake at western Sumatra of 2004 [35], the M7.9 Wenchuan earthquake of May 12, 2008 [20, 33], and M7.9 Haiti earthquake of January 12, 2010 [36]. The simultaneous occurrence of positive and negative TEC anomalies in magnetically conjugate EIA regions, together with distortion in EIA profile provides the strong evidence of seismo-ionospheric coupling prior the both earthquakes.

The conclusions of this study are based on two earthquake events; therefore, additional case studies are required to get more generalized results. In this work, only limited GNSS stations were available within EPZ, which may affect the spatial resolution of TEC observations. The inclusion of the more GNSS stations in future studies would provides improved spatial coverage and allow more comprehensive characterization of ionospheric variability.

The seismo-ionospheric coupling mechanism considered in this study is primarily interpreted within the framework of LAIC model, which involves processes such as radon emission and associated atmospheric ionization prior to earthquakes. However, alternative physical mechanisms, including electromagnetic emissions and acoustic–gravity wave propagation generated by lithospheric processes, have also been proposed to explain ionospheric disturbances preceding earthquakes [1, 2]. Distinguishing among these possible mechanisms remains challenging and requires multi-parameter observations, including atmospheric, electromagnetic, and satellite-based measurements.

4 Conclusions

Following are the major conclusions of this study.

- Analysis of ionospheric TEC from ground-based GNSS stations (BNOA and BTNG) reveals distinct anomalies before and after both earthquakes under geomagnetic quiet conditions.
- Spatiotemporal dTEC variation show positive anomalies occurring successively on the western and eastern sides of the epicenter, sepa-

rated by 2-3 days for two earthquakes. This behavior suggests reversal of atmospheric conductivity associated with air ionization due to radon emission from tectonic faults during the earthquake preparation phase.

- Negative TEC anomalies in magnetically conjugate regions are observed before both earthquakes, accompanied by morphological changes in EIA profile. These features are attributed to modification of background zonal electric field by earthquake-induced anomalous electric field.

Future investigations should include atmospheric and thermal/infrared parameters, such as relative humidity, air temperature, outgoing long wave radiation, etc., to further examine LAIC mechanism.

5 Acknowledgments

This work is supported by the University Grants Commission, Nepal, award number: **PhD-S&T-81/82-17**, under PhD fellowship award. We acknowledge the UNAVCO, USGS, Omni Web of NASA, ISGI and IGS for the public availability of the data.

References

[1] M. Hayakawa. Electromagnetic phenomena related to earthquake prediction. *Terra Sci. Pub. Comp., Tokyo*, 1994.

[2] M. Hayakawa. Electromagnetic phenomena associated with earthquakes: A frontier in terrestrial electromagnetic noise environment. *Recent Res. Devel. Geophysics*, 6; 81–112, 2004.

[3] S. Pulinets, A. Legen'Ka, T. Gaivoronskaya, and V. K. Depuev. Main phenomenological features of ionospheric precursors of strong earthquakes. *Journal of Atmospheric and Solar-Terrestrial Physics*, 65; 1337–1347, 2003. https://doi.org/10.1016/j.jastp.2003.07.011

[4] S. Pulinets, and K. Boyarchuk. Ionospheric Precursors of Earthquakes, Springer Science and Business Media, 2004. https://doi.org/10.1007/b137616

[5] S. Pulinets, A. Kotsarenko, L. Ciraolo, and I. Pulinets. Special case of ionospheric day-to-day variability associated with earthquake preparation. *Advances in Space Research*, 39; 970–977, 2007. https://doi.org/10.1016/j.asr.2006.04.032

[6] S. Pulinets, and D. Ouzounov. Lithosphere–Atmosphere–Ionosphere Coupling (LAIC) model–An unified concept for earthquake precursors validation. *Journal of Asian Earth Sciences* 41(4-5); 371-382, 2011. https://doi.org/10.1016/j.jseaes.2010.03.005

[7] S. Pulinets, and V. M. V. Herrera. Earthquake precursors: The physics, identification, and application. *Geosciences*, 14(8); 209, 2024. https://doi.org/10.3390/geosciences14080209

[8] J. Liu, Y. Chen, S. Pulinets, Y. Tsai, and Y. Chuo. Seismo-ionospheric signatures prior to M $\geq$ 6.0 Taiwan earthquakes. *Geophysical research letters*, 27(19); 3113-3116, 2000. https://doi.org/10.1029/2000GL011395

[9] G. E. Lanyi, and T. Roth. A comparison of mapped and measured total ionospheric electron content using global positioning system and beacon satellite observations. *Radio science*, 23(4); 483-492, 1988.

[10] J. Y. Liu, Y. Chuo, S. Shan, Y. Tsai, Y. Chen, S. Pulinets, and S. Yu. Pre-earthquake ionospheric anomalies registered by continuous GPS TEC measurements. *Annales Geophysicae* 22; 1585–1593, 2004. https://doi.org/10.5194/angeo-22-1585-2004

[11] J. Y. Liu, Y. Chen, C. H. Chen, C. Liu, C. Chen, M. Nishihashi, J. Li, Y. Xia, K. Oyama, K. Hattori, et al. Seismoionospheric GPS total electron content anomalies observed before the 12 may 2008 Mw7.9 Wenchuan earthquake. *Journal of Geophysical Research: Space Physics* 114, 2009. https://doi.org/https://doi.org/10.1029/2008JA013698

[12] J. Liu, C. Chen, Y. Chen, W. Yang, K. Oyama, and K. Kuo. A statistical study of ionospheric earthquake precursors monitored by using equatorial ionization anomaly of GPS TEC in Taiwan during 2001–2007. *Journal of Asian Earth Sciences*, 39; 76–80, 2010. https://doi.org/10.1016/j.jseaes.2010.02.012

[13] M. A. Tariq, M. Shah, M. Hernández-Pajares, and T. Iqbal. Pre-earthquake ionospheric anomalies before three major earthquakes by GPS-TEC and GIM-TEC data during 2015–2017. *Advances in Space Research*, 63; 2088–2099, 2019. https://doi.org/10.1016/j.asr.2018.12.028

[14] M. Shah, A. Ahmed, M. Ehsan, M. Khan, M. A. Tariq, A. Calabia, and Z. ur Rahman. Total electron content anomalies

associated with earthquakes occurred during 1998–2019. *Acta Astronautica*, 175; 268–276, 2020. https://doi.org/10.1016/j.actaastro.2020.06.005

[15] B. D. Ghimire and N. P. Chapagain. Ionospheric anomalies due to Nepal earthquake-2015 as observed from GPS-TEC data. *Geomagnetism and Aeronomy*, 62; 460–473, 2022. https://doi.org/10.1134/S0016793222040041

[16] A. Kiyani, M. Shah, A. Ahmed, H. H. Shah, S. Hameed, M. A. Adil, and N. A. Naqvi. Seismo ionospheric anomalies possibly associated with the 2018 mw 8.2 Fiji earthquake detected with GNSS-TEC. *Journal of Geodynamics*, 140; 101782, 2020. https://doi.org/10.1016/j.jog.2020.101782

[17] K. Nayak, C. López-Urías, R. Romero-Andrade, G. Sharma, G. M. Guzmán-Acevedo, and M. E. Trejo-Soto. Ionospheric total electron content (tec) anomalies as earthquake precursors: Unveiling the geophysical connection leading to the 2023 Moroccan 6.8 Mw earthquake. *Geosciences*, 13; 319, 2023. https://doi.org/10.3390/geosciences13110319

[18] Ryu, K., E. Lee, J. S. Chae, M. Parrot, and S. Pulinets. Seismo-ionospheric coupling appearing as equatorial electron density enhancements observed via DEMETER electron density measurements. *Journal of Geophysical Research: Space Physics*, 119; 8524–8542, 2014. https://doi.org/10.1002/2014JA020284

[19] Liu, J., Chen, C., Chen, Y., Yang, W., Oyama, K., and Kuo, K. A. Statistical study of ionospheric earthquake precursors monitored by using equatorial ionization anomaly of GPS TEC in Taiwan during 2001–2007. *Journal of Asian Earth Sciences*, 39(1–2); 76–80, 2010. https://doi.org/10.1016/j.jseaes.2010.02.012

[20] S. Pulinets, V. Bondur, M. Tsidilina, and M. Gaponova. Verification of the concept of seismoionospheric coupling under quiet heliogeomagnetic conditions, using the Wenchuan (China) earthquake of May 12, 2008, as an example. *Geomagnetism and Aeronomy*, 50(2), 231-242, 2010. https://doi.org/10.1134/S0016793210020118

[21] I. Dobrovolsky, S. Zubkov, and V. Miachkin. Estimation of the size of earthquake preparation zones Pure and Applied Geophysics 117, 1025–1044 (1979).

[22] T. Vincenty. Direct and inverse solutions of geodesics on the ellipsoid with application of nested equations. *Survey review*, 23(176); 88-93, 1975.

[23] R. Acharya. Understanding Satellite Navigation. Academic Press (2014). https://doi.org/10.1016/C2013-0-06964-2

[24] J. A. Klobuchar, Ionospheric time-delay algorithm for single frequency GPS users. *IEEE Transactions on aerospace and electronic systems*, 325–331, 1987.

[25] G. K. Seemala. Estimation of ionospheric total electron content (tec) from GNSS observations. *Atmospheric remote sensing*, Elsevier, pp. 63–84, 2023. https://doi.org/10.1016/B978-0-323-99262-6.00022-5

[26] J. Y. Liu, Y. Chen, Y. Chuo, and C. S. Chen. A statistical investigation of pre-earthquake ionospheric anomaly. *Journal of Geophysical Research: Space Physics*, 111, 2006. https://doi.org/10.1029/2005JA011333

[27] N. Balakrishnan, and N. Johnson, Samuel Kotz. Continuous Univariate Distributions. Vol. 1, *John Wiley & Sons, Inc*, 1994.

[28] W. Gonzalez, J. A. Joselyn, Y. Kamide, H. W. Kroehl, G. Rostoker, B. T. Tsurutani, and V. Vasyliunas. What is a geomagnetic storm? *Journal of Geophysical Research: Space Physics*, 99(A4); 5771-5792, 1994.

[29] H. Rishbeth, and M. Mendillo. Patterns of F2-layer variability. *Journal of Atmospheric and Solar-Terrestrial Physics*, 63(15); 1661-1680, 2001. https://doi.org/10.1016/S1364-6826(01)00036-0

[30] L. Liu, W. Wan, B. Ning, O. M. Pirog, and V. I. Kurkin. Solar activity variations of the ionospheric peak electron density. *Journal of Geophysical Research: Space Physics*, 111; A08304, 2006. https://doi.org/10.1029/2006JA011598

[31] K. F. Tapping. The 10.7 cm solar radio flux (F10. 7). *Space Weather*, 11(7); 394-406, 2013. https://doi.org/10.1002/swe.20064

[32] J. Matzka, O. Bronkalla, K. Tornow, K. Elger, and C. Stolle. Geomagnetic Kp index. *GFZ Data Services*, 2021. https://doi.org/10.5880/Kp.v0001

[33] S. Pulinets. Low-latitude atmosphere-ionosphere effects initiated by strong earthquakes preparation process. *International Journal of Geophysics*, 2012(1); 131842, 2012. https://doi.org/10.1155/2012/131842

[34] L. Cullen, A. W. Smith, A. H. Galib, D. Varshney, E. J. Brown, P. J. Chi, ... , and F. Svoboda. A Global Analysis of Pre-Earthquake Ionospheric Anomalies. arXiv preprint arXiv:2401.01773, 2024.

[35] I. E. Zakharenkova, A. Krankowski, and I. I. Shagimuratov. Modification of the low-latitude ionosphere before the 26 December 2004 Indonesian earthquake. *Natural Hazards and Earth System Sciences*, 6(5); 817-823, 2006. https://doi.org/10.5194/nhess-6-817-2006

[36] S. Pulinets, and K. G. Tsybulya. Unique variations of the total electron content in the preparation period of Haitian earthquake (M7.9) on January 12, 2010. *Geomagnetism and Aeronomy*, 50(5); 686-689, 2010. https://doi.org/10.1134/S0016793210050166